Extension and Limits of Cryoscopy for Nanoconfined Solutions

Benjamin Malfait, Alban Pouessel, Aicha Jani, Denis Morineau

▶ **To cite this version:**

Benjamin Malfait, Alban Pouessel, Aicha Jani, Denis Morineau. Extension and Limits of Cryoscopy for Nanoconfined Solutions. Journal of Physical Chemistry Letters, 2020, 11 (14), pp.5763-5769. 10.1021/acs.jpclett.0c01564 . hal-02883916

HAL Id: hal-02883916
https://hal.science/hal-02883916

Submitted on 3 Jul 2020

HAL is a multi-disciplinary open access archive for the deposit and dissemination of scientific research documents, whether they are published or not. The documents may come from teaching and research institutions in France or abroad, or from public or private research centers.

L'archive ouverte pluridisciplinaire **HAL**, est destinée au dépôt et à la diffusion de documents scientifiques de niveau recherche, publiés ou non, émanant des établissements d'enseignement et de recherche français ou étrangers, des laboratoires publics ou privés.

Extension and Limits of Cryoscopy for Nanoconfined Solutions

Benjamin Malfait,[†] Alban Pouessel,[†] Aîcha Jani,[†] Denis Morineau[†*]

[†]Institute of Physics of Rennes, CNRS-University of Rennes 1, UMR 6251, F-35042 Rennes, France

Corresponding Author

* Email: denis.morineau@univ-rennes1.fr

This work investigates the phase behavior of aqueous solutions of glycerol confined in MCM-41 and SBA-15 nanoporous matrixes by calorimetry. Limitations due to overfilling and eutectic freezing are prevented by the absence of an external liquid reservoir and by the glassforming property of glycerol. Consequently, the stability of nanoconfined ice in equilibrium with aqueous solutions is studied over a wide range of compositions. In confinement, a large temperature depression of the liquidus line is observed. A thermodynamic model accounting simultaneously for the cryoscopic and the Gibbs-Thomson effects gives a consistent view of the phase diagram for large pores (R_p = 4.15 nm). For smaller pores (R_p = 1.8 nm), it reveals that the water activity strongly deviates from the bulk solution with the same composition, indicating the possible role of concentration heterogeneities in determining the onset of ice freezing in strongly nanoconfined solutions.

TOC GRAPHIC

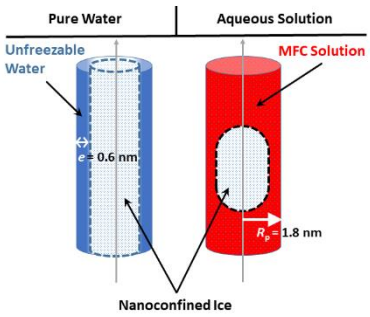
Pure Water
Aqueous Solution
Unfreezable Water
MFC Solution
e = 0.6 nm
R_p = 1.8 nm
Nanoconfined Ice

The lowering of the melting point of frozen liquids by the addition of a solute is a fundamental and well-established phenomenon. Its early study by Bernoulli dates back to the eighteenth century.[1] The linear relation between the melting depression and the amount of salts dissolved in water, usually known as the Blagden's law was proposed in 1788.[2] About one century later, this prediction was extended to different systems, including organic and inorganic solvents and solutes. This phenomenon was established as one of the three Raoult's laws, which embrace the overall colligative properties of solutions.[3]

The melting point depression of aqueous solutions induced by solutes, such as inorganic salts or alcohols serves many important applications.[4] Fundamentally, it is the basis of cryoscopy and a related method, which was used to determine the molar mass and degree of ionic dissociation of solutes.[5] It also has many practical uses such as road salting in winter, the formulation of anti-freezing additives (e.g. ethylene glycol) in the radiators of cars, or cryoprotectant agents (e.g. glycerol, trehalose) for the safe storage and manipulation of food, pharmaceutical and medical materials.[6, 7] This phenomenon also profits to living organisms, which produce natural solutes with a high biopreservative action (e.g. sugars, polyols) in order to adapt to severe icy conditions.[8] The exceptional melting point reduction achieved by mixing H-bonded molecules is also at the basis of the very promising family of alternative solvents, known as deep eutectic solvents.[9-11]

When they are spatially confined at the nanometer scale, many fundamental properties of the liquid states are also modified. Experimental and molecular simulation studies on various types of solvents embedded in nanoporous matrixes have reported large confinement effects on the phase behavior, structure and molecular dynamics.[12-23] In this context, the significance of cryoscopy as

well as the colligative nature of the freezing point depression by addition of solutes must be reconsidered in nanoconfined geometry.

At present, only a few studies are available in the literature and apparently contradicting behaviors were observed, some studies indicating no cryoscopic effect in confinement, and others indicating enhanced cryoscopic effects.

On the one hand, it has been shown that the melting point of confined solutions was basically independent on the initial solute concentration in two studies that addressed solutions of different nature (benzene-cyclohexane mixtures in SBA-15 silicates,[24] and series of alkali halides solutions in MCM-41 and SBA-15 silicates[25]). In both cases, the authors demonstrated that this constant temperature was in fact related solely to the eutectic point, and not to the liquidus line.

One the other hand in the limit of high dilution, an enhancement of the cryoscopic effect under confinement was shown for NaCl solutions in SBA-15 and MCM-41[26] and benzene-toluene mixtures in SBA-15.[27] The former study was complemented by Jantsch *et al.* in the range of higher concentrations for $CaCl_2$ and LiCl solutions confined in SBA-15 and MCM-41 mesoporous silicates.[28] The combined effects of confinement and the presence of solutes were accounted for by an effective activity, in which the solute effect at ambient pressure and the Kelvin pressure effect were estimated independently. Although satisfying for the largest pore sizes of the SBA-15 materials (R_p > 5 nm), this classical thermodynamic approach failed to understand observations made for smaller pore size, where no concentration dependence on the ice melting was observed. This observation was attributed to the exclusion of ions from small pores.[28]

As a whole, the phase behavior of confined solutions and binary liquids remains unclear. This is especially relevant for pore sizes of only a few nanometers (i.e. R_p < 5 nm) where experimental

observations of the liquidus line are missing, since existing studies were either restricted to the limit of high dilution or unrelated to the liquidus line itself because of eutectic freezing and solute exclusion.[25, 26, 28] Besides, other specific phenomena have been invoked to interpret experimental observations in the presence of excess liquid, such as the variation of the ice-liquid surface tension as a function of the composition,[26] the unexpected exclusion of ions from small pores,[28] the effects of secondary confinement or the precipitation of solute nanocrystals.[25]

In this Letter, we argue that a necessary condition of access to the liquidus line in porous media, which prevents from the intervention of other physical phenomena, lies in the actual control of the composition of the confined solution. This point has not received sufficient attention so far. In fact, to the best of our knowledge, the existing studies implied an external reservoir of excess liquid so that the liquid composition in the pores was allowed to vary with temperature, as demonstrated experimentally.[24, 25] This effect was thoroughly explained by Findenegg *et al*.[25] In this study, they argued that during cooling, the external reservoir crystallizes first, and this increases the solute concentration of the remaining excess liquid, which is in equilibrium with the confined fluid. As a consequence, the concentration of the confined liquid also increases before it crystallizes. For diluted systems, we infer that this drift of the concentration of the confined liquid could lead to the apparent enhanced cryoscopic effect in the confined state.[26, 27] At variance for concentrated systems, because the solute is also expected to crystallize, the variation of concentration of the confined solution during cooling is finally bounded by the bulk eutectic composition, before freezing starts in the pores. In this case, no information on the liquidus line can be attained either. Indeed, as argued by the authors of these two studies, both the composition and the melting temperatures of the confined system are determined by the eutectic point and appear independent on the initial mixture composition.[24, 25]

In this Letter, we report on a study aiming at revealing the confinement effects on the liquidus line and thus the cryoscopic properties of aqueous solutions by selecting, for the first time, a set of conditions which fulfill two important prerequisites: First, a temperature invariant composition of the confined liquid, implying pore filling with no excess-liquid. Second, the absence of any solute precipitate over the widest range of concentration, from the dilute to the highly (pure) concentrated regime. The later condition means that the solute can be maintained easily in its supercooled liquid state so that solute precipitation and eutectic freezing is fully avoided. Under these conditions, we could unravel experimental evidences of the limits of cryoscopy at the nanoscale.

For this purpose, we chose glycerol as a solute instead of ionic salts. Glycerol has been extensively used as a cryoprotectant, and as a prototypical glassforming liquid, its crystallization could be easily avoided in normal conditions.[29-31] The phase diagram of water-glycerol solutions confined in the well-defined cylindrical pores of MCM-41 and SBA-15 silicates (pore radius R_P = 1.8 and 4.15 nm) was determined by DSC. The exact value of the composition of the confined aqueous solution, ranging from pure water to pure glycerol, was reached by a careful control of the filling fraction and the confirmed absence of any thermal event due to a hypothetical excess liquid as demonstrated in the Supporting Information.

The phase behavior of glycerol aqueous solutions has been extensively studied in the bulk state.[32-35] Glycerol has a pronounced tendency to supercool in normal conditions, and seeding is usually required to induce crystallization.[32] The two equilibrium liquidus lines that cross at an eutectic point (glycerol mass fraction W_G^E = 66.7%, and T_E = 226.65 K) are shown in Figure S1a. Without seeding, only water normally crystallizes during cooling, which leads to the different phase diagram as shown in Figure S1b, which combined data from the literature and additional data acquired in this study with corresponding thermograms provided in Figure S2 and S3. For

large mass fractions of glycerol (W_G > 70%) the entire solution can be supercooled and it forms a glassy state at the temperature T_g. For small fractions of glycerol (W_G < 45%), ice forms on cooling, while the co-existing freeze-concentrated aqueous solution remains disordered (liquid or glassy). This was also confirmed by our measurement for W_G = 30% illustrated in Figure S2, where the crystallization is indicated by the endothermic peak at *T*c. On heating, according to the many studies on glycerol solutions, including the most recent work by the group of Loerting, the first thermal event at T_g' is attributed to the glass transition of the maximally-freeze-concentrated (MFC) solution.[33-37] The melting of ice occurs on an extended temperature range. At low temperature, the onset of melting depends on the activity of water in the MFC solution, while the last crystallites melt at a temperature T_m fixed by the activity of water in the entirely melted solution. We referred to T_m as the liquidus, and to T_m' as the onset of freezing, noting also that the latter event can be additionally affected by "interface ice" effects and the combination of "cold recrystallization/ice dissolution as discussed in the litterature.[34, 35] In the intermediate region (45% < W_G < 70%), both situations (ice formation or not) occur depending on the thermal treatment, allowing the independent determination of T_g and T_g'. This is illustrated by our measurement for W_G = 60% in Figure S3.

The DSC thermograms acquired during the heating ramp as a function of the temperature and the glycerol mass fraction are illustrated in Figures 1a and 1b, for the solutions confined in the SBA-15 and the MCM-41, respectively. For completeness, enlarged views of the different individual thermograms acquired on heating and on cooling are provided in Supporting Information (Figures S4, S5, S6 and S7). It is worth pointing out that crystallization is a more complex phenomenon than melting because it is affected by supercooling and implies different processes such as nucleation and growth. For pure water confined in SBA-15, it was shown that

ice formation implied up to three exothermic peaks, but only a single endothermic event on melting.[38] We made similar observation for the thermograms of the confined solutions on cooling (Figure S4). It is also noteworthy that in SBA-15, the onset of crystallization shifted to lower temperature on increasing the amount of glycerol, and exhibited significant thermal hysteresis. At variance in MCM-41, the crystallization was weakly dependent on W_G and the thermal hysteresis was virtually absent. This observation of the disappearance of the thermal hysteresis in small pores extends previous conclusions made for pure water.[38]

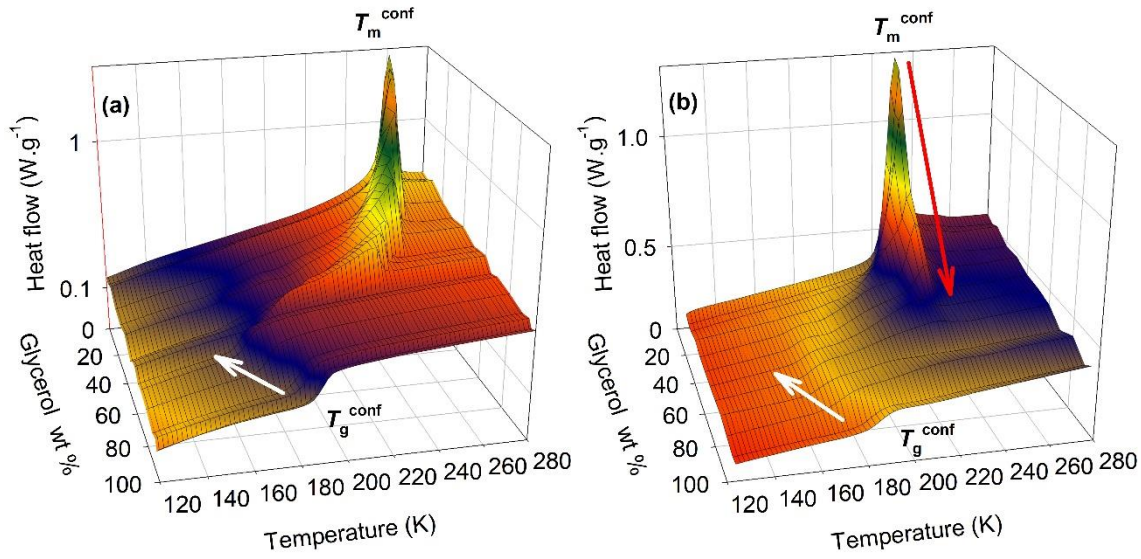

Figure 1. Thermograms of the glycerol – water binary mixture confined in (a) SBA-15 and in (b) MCM-41 as a function of the temperature and the glycerol mass fraction. The endothermic heat flow points upward and the heating ramp was 5 K.min^{-1}. On the glycerol-rich side of the phase diagram, the shift to lower temperature of the glass transition as a function of the glycerol mass fraction is underlined by a white arrow. On the water-rich side of the phase diagram, the reduction

of the amount of ice that melted at a barely varying temperature for MCM-41 is underlined by a red arrow.

Due to these effects of metastability, the scans on cooling are not appropriate to obtain reliable information on the liquidus. The scans acquired on heating have been used instead, including thermal cycling for W_G=60% as also done for the bulk. They are illustrated in Figures S6, S7, and S8. The behaviors obtained in the porous matrixes were qualitatively similar to those of the bulk solutions, and are summarized in Figure 1 by a 3D plot of all the thermograms acquired on warming.[33-37] This similarity is due to the tendency of ice to crystallize in mesopores, which is no more the case in micropores (i.e. R_p = 1.0 nm).[39] On the quantitative level however, large differences were observed between the three systems concerning the melting temperatures and their dependence on the glycerol composition.

This is illustrated in Figure 1 by a heat capacity jump at the glass transition temperature T_g for glycerol-rich mixtures. For water-rich mixtures, we observed the coexistence of the broad endothermic melting peak of ice with a maximum located at T_m and the glass transition temperature of the maximally-freeze-concentrated (MFC) solution T_g'. The transition temperatures of the different systems are compared in Figure 2. The composition of the MFC solution W'_G is barely dependent on the initial composition of the solution and it is therefore straightforward that for $W < W'_G$, provided that ice crystallization occurs, this composition determines the value of the glass transition T_g'.[36, 40] This is illustrated in Figure 2, by identifying W'_G as the composition where the extrapolated value of T_g' crosses T_g. The composition of the MFC solution could also be evaluated from the extrapolation to zero of the melting enthalpy, as also done in the literature and illustrated in Figure S9. [40, 41] Applying these two commonly used methods, we obtained constituent values

of $W_G' \approx 70\%$ for the confined systems. Within experimental uncertainties, they appeared similar to the value reported for the bulk solution $W_G' = 75\%$.[36]

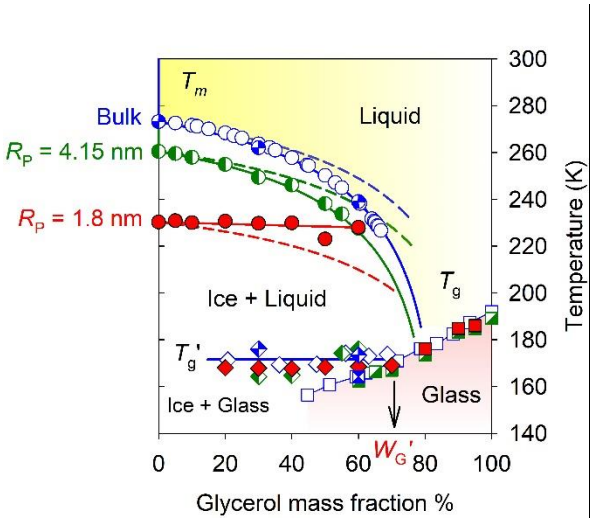

Figure 2. Phase diagram of the glycerol – water binary mixture in the bulk state, including data from the literature (open symbols) and from the present study (hourglass symbols), confined in SBA-15 (half-filled symbol) and confined in MCM-41 (filled symbol) as a function of the mass fraction of glycerol. The experimental liquidus (circles), the glass transition temperatures of the homogenous aqueous solution T_g (squares), and the maximally freeze concentrated solution T_g' (diamonds). The theoretical predictions from extended Gibbs-Thomson equation with ideal mixing (eq. 4, short dashed line). Solid lines are guides to the eyes. The bulk liquidus, T_g and T_g' are extracted from ref. 32, 33, and 34.

We now consider the ultimate goal of this study on a quantitative level, which is to resolve the confinement effect on the liquidus line illustrated in the phase diagram presented in Figure 2. In confinement, we observed a reduction of T_m^{conf} with respect to T_m^{Bulk}, which evokes the well-known confinement effect on the melting point of pure compounds, as usually named the *Gibbs-Thomson effect*. Moreover, we observed an additional depression of T_m^{conf} as a function of glycerol

mass fraction W_G , as denoted the *cryoscopic effect*. However, this cryoscopic effect is much reduced for the smallest pore radius, being only a few degrees for R_p = 1.8 nm, compared to a few tens of degrees for both the bulk and for largest pore radius R_p = 4.15 nm.

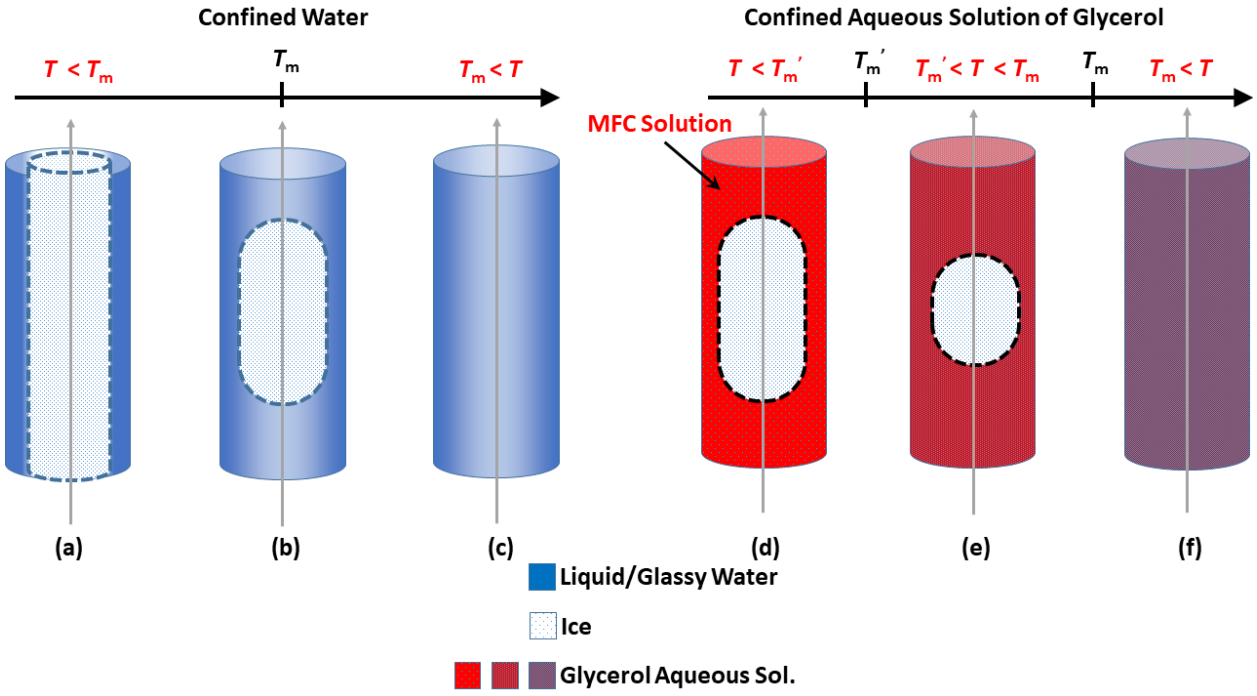

Figure 3. Sketch of the confined water and aqueous solution in different region of the phase diagram.

The thermodynamics of the confined system illustrated in Figure 3 can be expressed by the Gibbs energy of a cylindrical ice crystal composed of n_s water molecules, in contact with a liquid solution of solute molar fraction *x* under full wetting condition (cf. Supporting Information), which writes as

$$G_s(T, n_s) = n_s\mu_s(T) + 2\frac{n_s v_s}{r}\gamma_{sl} + 2\pi r^2\gamma_{sl} \qquad (1)$$

with *r* the radius of the crystal, $v_s$is the molar volume of water in ice, μ_i the chemical potential of phase *i* (*i* = *s*, *l* for solid ice and liquid), and γ_{sl} the ice-solution surface energy.

The melting temperature T_r^x of the confined ice is determined by the equilibrium condition between the solid and the liquid solution, which implies that

$$\left(\frac{\partial G_s}{\partial n_s}\right) = \left(\frac{\partial G_l}{\partial n_l}\right) \qquad (2)$$

and so

$$\mu_s(T_r^x) - \mu_l(T_r^x, x) = -\frac{2\,v_s\gamma_{sl}}{r} \qquad (3)$$

In order to deduce the melting temperature T_r^x by solving eq 3 the knowledge of $\mu_l(T, x)$ and γ_{sl} is required. This is straightforward if one makes the further assumptions that (a) the variation with *T* and *x* of the solid-liquid surface energy is negligible, (b) the solution fulfills the ideal mixing approximation, and (c) the heat capacity contribution to the bulk water Gibbs energy difference is small compared to the melting enthalpy term ΔH_m (cf. Supporting Information). The two latter assumptions are used in the classical derivations of the Raoult's law and Gibbs-Thomson equation respectively.

The melting point of ice T_r^x writes then as an *extended version of the Gibbs-Thomson equation*

$$T_r^x - T_{bulk}^0 = \frac{-2\gamma_{sl}v_s T_{bulk}^0}{\Delta H_m r} + \frac{RT_r^x\, T_{bulk}^0 \ln(1-x)}{\Delta H_m} \qquad (4)$$

with *x* being the glycerol molar fraction, ΔH_m the bulk ice melting enthalpy and *R* the gas constant.

Interestingly, the right side of eq 4 comprises two terms, which reflect the cumulative effects of confinement and solute on the ice melting point depression.

For pure water (x = 0), one recovers the *classical Gibbs-Thomson equation*

$$T_r^0 - T_{bulk}^0 = \frac{-2\gamma_{sl}v_s T_{bulk}^0}{\Delta H_m r} \qquad (5)$$

which is in perfect agreement with the experimental values (Table 1 in Supporting Information) if one assumes an interfacial layer of unfreezable liquid of thickness e = 0.6 nm, so that $r = R_p - e$, and the value of the Gibbs-Thomson constant $C_{GT} = \frac{2\gamma_{sl}T_{bulk}^0}{\Delta H_m \rho_s} = 52.4\ K.nm$ in accordance with Findenegg.[38] It should be noted that there are ongoing discussions about the nature of confined ice (hexagonal/cubic, stacking disordered).[42] Our calculation is based on the values (T_{bulk}^0 and ΔH_m) of the bulk (hexagonal) ice phase. This choice is in line with the widely used methods of thermoporosity, and is also supported by the quantitative agreement obtained for pure water.

For the aqueous solutions, the predictions from eq 4 are shown as short dashed lines in Figure 2. For the SBA-15, the experimental cryoscopic depression of T_r^x is larger than predicted. However, the level of disagreement is very similar to that already observed for the bulk solution (open and hourglass circles). It is thus reasonable to attribute it to a same origin. Regarding the three approximations made, it means that invoking the hypothetical variation of γ_{sl} is not needed in the present study and that most probably, the ideal mixing approximation is the main limitation to the model.

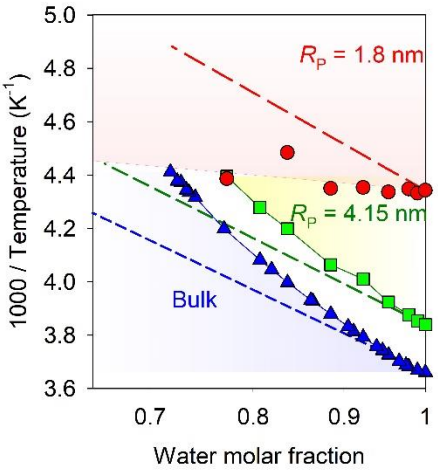

Figure 4. Inverse melting temperature as a function of the water molar fraction (logscale) of the glycerol – water binary mixture bulk (triangle), confined in SBA-15 (square) and in MCM-41 (circle). The theoretical predictions based on the extended cryoscopic equation with ideal mixing (eq. 6, dashed line).

Under the same level of approximation, we removed the explicit references to γ_{sl} and to the ice radius *r* (cf. Supporting Information) and derived the *extended cryoscopic equation* with ideal mixing

$$\frac{1}{T_r^x} - \frac{1}{T_r^0} = -\left(\frac{T_{bulk}^0}{T_r^0}\right)\frac{R\ln(1-x)}{\Delta H_m} \qquad (6)$$

where all the effects of confinement are implicitly contained in the melting point temperature of pure water T_r^0. For bulk water ($T_r^0 = T_{bulk}^0$), one recovers the *classical cryoscopic* equation

$$\frac{1}{T_{bulk}^x} - \frac{1}{T_{bulk}^0} = -\frac{R\ln(1-x)}{\Delta H_m} \qquad (7)$$

According to eq 6, the effect of adding a solute on the inverse melting point variation should be larger for a confined system than for the bulk since it scales with $\frac{T_{bulk}^0}{T_r^0} > 1$, the latter coefficient being a consequence of the Gibbs-Thomson confinement effect for the pure water.

This model actually gave a quantitative prediction of the asymptotic variation of T_r^x in the dilute regime for R_p = 4.15 nm and for the bulk (solute molar fraction lower than 5%), as illustrated by Figure 4. In the more concentrated regime, deviations from a linear cryoscopic variation were observed, which obviously underlines the breakdown on the ideal mixing approximation for aqueous solutions. Contrariwise, for R_p = 1.8 nm the *extended cryoscopic* equation failed to reproduce the weak dependence of T_r^x on the mixture composition, even in the limit of highly diluted system where non-ideality effects are usually reduced. It means that in small pores, other effects than the simple deviation of aqueous solutions from the ideal mixing approximation must be present.

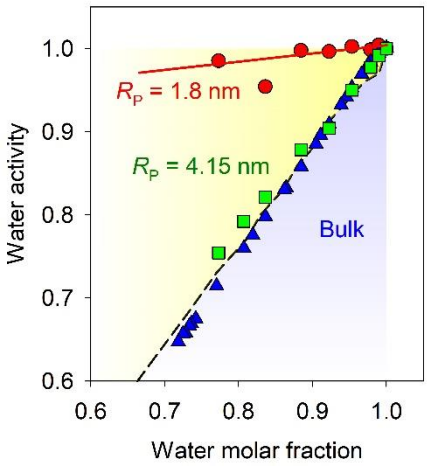

Figure 5. Water activity as a function of the water molar fraction of the glycerol – water binary mixture bulk (triangle), confined in SBA-15 (square) and in MCM-41 (circle), obtained from the

experimental values of the melting points and using an extended cryoscopic model with non-ideal mixing (eq. 8). It is computed with the experimental Gibbs energy for pure water from ref. [43]. Water activity of glycerol – water binary mixture derived from the vapor pressure at 25°C (dashed line) from ref. [44].

In order to gain a better insight, it is worth coming back to the initial expression of the Gibbs energy (eq 3), with a better degree of approximation. In the following, we only retained the assumption that (a) the variation of γ_{sl} is negligible as justified previously, while the non-ideal character of mixing was included, and the precise chemical potential of water was obtained from a detailed consistent thermodynamic integration of calorimetric data.[43] Under these minimal hypothesis, the activity of water in the confined solution could be evaluated with eq 8, (cf. Supporting Information) based on the experimental values of the melting point temperature of the confined solution T_r^x , and the pure water T_r^0 , with $\Delta\mu_0(T)$ being the difference in the chemical potential between ice and liquid pure bulk water, determined by Johari [43] in a temperature range from 273,15 to 153K and later parametrized by Koop et al. [45]

$$a(r, T_r^x, x) = Exp\left\{\frac{\Delta\mu_0(T_r^x) - \Delta\mu_0(T_r^0)}{R\,T_r^x}\right\} \qquad (8)$$

The values of the water activity obtained from eq 8 are presented in Figure 5. They are also compared with a different evaluation of the water activity, defined classically as the ratio of the vapor pressure of water in equilibrium with a water-glycerol solution to the saturation vapor pressure of pure water at 25°C.[44] For bulk solutions, an excellent agreement was obtained between the activity derived from the melting point and from the vapor pressure, with a clear demonstration of the systematic deviation from the ideal mixing approximation ($a = x$). In the SBA-15, the water activity of the confined solution obtained from eq 8 seemed also to conform nicely to the bulk

values. A possible tiny deviation from this bulk-like behavior could be hardly confirmed in the concentrated regime within experimental uncertainties. On the contrary, a clear breakdown of this bulk-like behavior occurred for the smaller pore size in the MCM-41, where the activity of water in the confined mixtures exhibited a much weaker dependence on the solute concentration.

Interestingly, the liquidus line can be viewed as the melting temperature T_m^{conf} of the tiniest fraction of ice that remains in the nanoconfined solution, when all the rest of the freezable water has already melted. From this viewpoint, our results suggest that the composition of the solution, which determines through its water activity the value of T_m^{conf} is different from the average composition of the entire solution. However at lower temperature, when the entire fraction of freezable confined water has formed ice, the composition of the maximally freeze-concentrated solution agrees well with the bulk value ($W_G' \approx 70\%$). We argue that this indicates that local heterogeneities of concentration are involved, and that they trigger the position of the liquidus, which cannot be explained solely by the average composition of the whole confined liquid. This conclusion is the main novelty with respect to the existing literature. Indeed in previous studies, the concentration of the whole confined solution was expected to vary on approaching the liquidus line because of eutectic freezing, solute precipitation, solute rejection and the presence of an extra reservoir of liquid.[24-28] On the contrary, the glassforming ability of glycerol demonstrates that the eutectic point did not play any role. The fact that the whole composition of the confined liquid at T_m^{conf} could be different from the mother solution due to external ice freezing[25] or to the solutes exclusion from the pores[28] can be also safely ruled out in this study. First, it was shown that all the ice was actually confined in the pore. This condition was realized by the absence of a reservoir of excess solution, and confirmed by the nonappearance of any thermal signature of bulk melting, and by the large depression of T_m^{conf}. Second, the systematic broadening of the low-temperature

side of the melting peak of the confined ice and the formation of the maximally freeze-concentrated solution ($W'_G \approx 70\%$) implied that the nanoconfined ice was interacting with the remaining glycerol aqueous solution, the latest being also present in the pores. In other words, there was no sign of solute exclusion.

In conclusion, we have shown that an *extended Gibbs-Thomson equation*, or *extended cryoscopic equation* assuming ideal mixing, gave an appropriate description of the phase behavior of confined glycerol aqueous solution, provided that the pore size is large enough (R_p = 4.15 nm). In this case, the Gibbs-Thomson effect was dominant, and the cryoscopic effect could be quantitatively reproduced assuming that the activity of water in the confined solution was comparable to that of the bulk at the same composition. Strikingly, for a smaller pore (R_p = 1.8 nm), the phase behavior indicated that the end of melting on heating and also the onset of freezing on cooling were determined by a very different water activity, which exhibited a much weaker dependence on the solute concentration. We consider that the conditions used in the present study allowed us to refute other interpretations that have been previously invoked in studies influenced by eutectic freezing, in-pore concentration variation and outer-pore excess liquid. Instead, this study underlines the inhomogeneous character of the nanoconfined aqueous solution. It is worth mentioning that microphase separation phenomena induced by nanoconfinement and interfacial interaction have been reported for different binary liquid mixtures based on dynamical information.[39, 46-48] Moreover, direct structural evidences were also obtained from neutron scattering methods and molecular simulation.[49-51] The microphase segregation facilitating ice formation in water-rich domains was also invoked to rationalize the enhanced tendency for partial crystallization for glycol-water mixtures.[52] However, the relation between microphase segregation and the phase diagram of nanoconfined solutions has not been determined on a qualitative level so

far. This Letter suggests that water-rich nanoregions, and not the average concentration of the solution, determine the liquidus line, and the onset of crystallization as well. At temperature below the liquidus line, ice further invades the matrix porosity. We showed that this growth of crystals performs in interaction with a confined freeze-concentrated solution. This is demonstrated by the large depression of the onset of melting with respect to the liquidus -and likewise the extension to lower temperature of the freezing process on cooling. The fraction of ice is finally limited by the formation of a nanoconfined maximally freeze-concentrated solution, with a composition that is reminiscent of the bulk one. To our best knowledge, this Letter provides the first evidence of a link between water microsegregation and the liquid-solid phase diagram in nanoconfined solutions. It brings a new insight on a topics founded on two fundamental pillars of the thermodynamics of condensed matter physics (i.e. the Blagden and Raoult's law of cryoscopy and the Gibbs-Thomson effect) and how their combined effects could reveal new phenomena in aqueous solutions confined at the nanoscale. It indicates that their possible impacts in many applied fields of confined solutions should be carefully scrutinized in the future.

ASSOCIATED CONTENT

Supporting Information

Phase diagram of bulk glycerol-water solutions with and without crystal seeding. DSC thermograms on heating and cooling of two bulk solutions and all the solutions confined in MCM-41 and SBA-15. Melting enthalpy of confined glycerol-water solutions. Effect of thermal cycling on the DSC thermograms of glycerol-water solution (W_G=60%) in the bulk state and confined in SBA-15. Effects of a reservoir of excess bulk liquid on the DSC thermograms of confined glycerol-water solutions. Control of the filling fraction. Detailed derivation of the thermodynamic theoretical models used in the study. Predictions of the melting temperature of pure ice confined

in SBA-15 and MCM-41 using the classical Gibbs-Thomson equation (Table S1). Materials and methods. Related references.

ACKNOWLEDGMENTS

Support from Rennes Metropole and Europe (FEDER Fund – CPER PRINT2TAN), and the ANR (Project NanoLiquids N° ANR-18-CE92-0011-01) is expressly acknowledged. This work is part of the Ph.D. thesis of A.J. who benefits from a grant from the French Ministry of Higher Education, Research, and Innovation. We thank Odile MERDRIGNAC (Institut des Sciences Chimiques de Rennes) for her assistance with Nitrogen isotherms experiments for the characterization of the MCM-41 and SBA-15 materials.

REFERENCES:

1. Reif-Acherman, S., The Pre-History of Cryoscopy: What was Done before Raoult? *Quimica Nova* **2009,** *32* (6), 1677-1684.

2. Blagden, C., Experiments on the Effect of Various Substances in Lowering the Point of Congelation in Water. By Charles Blagden, M. D. Sec. R. S. and F. A. S. *Philosophical Transactions of the Royal Society of London* **1788,** *78*, 277-312.

3. Raoult, F. M., Sur le Point de Congélation des Liqueurs Alcooliques. *Comptes Rendus de l'Académie des Sciences* **1880,** *90*, 865-868.

4. Angell, C.; Bressel, R.; Green, J.; Kanno, H.; Oguni, M.; Sare, E., Liquid Fragility and the Glass-Transition in Water and Aqueous-Solutions. *Journal of Food Engineering* **1994,** *22* (1-4), 115-142.

5. Gerold, A.; Jastrzebski, J.; Kronenburg, C.; Krause, N.; vanKoten, G., Determination of the Degree of Aggregation of Organocopper Compounds by Cryoscopy in Tetrahydrofuran. *Angewandte Chemie-International Edition in English* **1997,** *36* (7), 755-757.

6. Rall, W.; Fahy, G., Ice-Free Cryopreservation of Mouse Embryos at -196-Degrees-C by Vitrification. *Nature* **1985,** *313* (6003), 573-575.

7. Berendsen, T.; Bruinsma, B.; Puts, C.; Saeidi, N.; Usta, O.; Uygun, B.; Izamis, M.; Toner, M.; Yarmush, M.; Uygun, K., Supercooling Enables Long-Term Transplantation Survival Following 4 Days of Liver Preservation. *Nature Medicine* **2014,** *20* (7), 790-793.

8. Bale, J.; Hayward, S., Insect Overwintering in a Changing Climate. *Journal of Experimental Biology* **2010,** *213* (6), 980-994.

9. Abbott, A.; Boothby, D.; Capper, G.; Davies, D.; Rasheed, R., Deep Eutectic Solvents formed between Choline Chloride and Carboxylic Acids: Versatile Alternatives to Ionic Liquids. *Journal of the American Chemical Society* **2004,** *126* (29), 9142-9147.

10. Zhang, Q.; Vigier, K.; Royer, S.; Jerome, F., Deep Eutectic Solvents: Syntheses, Properties and Applications. *Chemical Society Reviews* **2012,** *41* (21), 7108-7146.

11. Ge, X.; Gu, C.; Wang, X.; Tu, J., Deep Eutectic Solvents (DESs)-Derived Advanced Functional Materials for Energy and Environmental Applications: Challenges, Opportunities, and Future Vision. *Journal of Materials Chemistry a* **2017,** *5* (18), 8209-8229.

12. Jackson, C. L.; McKenna, G. B., The Melting Behavior of Organic Materials Confined in Porous Solids. *Journal of Chemical Physics* **1990,** *93* (12), 9002-9011.

13. Jackson, C.; McKenna, G., The Glass-Transition of Organic Liquids Confined to Small Pores. *Journal of Non-Crystalline Solids* **1991,** *131*, 221-224.

14. Granick, S., Motions and Relaxations of Confined Liquids. *Science* **1991,** *253* (5026), 1374-1379.

15. Christenson, H. K., Confinement Effects on Freezing and Melting. *Journal of Physics-Condensed Matter* **2001,** *13* (11), R95-R133.

16. Morineau, D.; Xia, Y. D.; Alba-Simionesco, C., Finite-Size and Surface Effects on the Glass Transition of Liquid Toluene Confined in Cylindrical Mesopores. *Journal of Chemical Physics* **2002,** *117* (19), 8966-8972.

17. Alba-Simionesco, C.; Dosseh, G.; Dumont, E.; Frick, B.; Geil, B.; Morineau, D.; Teboul, V.; Xia, Y., Confinement of Molecular Liquids: Consequences on Thermodynamic, Static and Dynamical Properties of Benzene and Toluene. *European Physical Journal E* **2003,** *12* (1), 19-28.

18. Alcoutlabi, M.; McKenna, G. B., Effects of Confinement on Material Behaviour at the Nanometre Size Scale. *Journal of Physics-Condensed Matter* **2005,** *17* (15), R461-R524.

19. Alba-Simionesco, C.; Coasne, B.; Dosseh, G.; Dudziak, G.; Gubbins, K. E.; Radhakrishnan, R.; Sliwinska-Bartkowiak, M., Effects of Confinement on Freezing and Melting. *Journal of Physics-Condensed Matter* **2006,** *18* (6), R15-R68.

20. Kityk, A. V.; Wolff, M.; Knorr, K.; Morineau, D.; Lefort, R.; Huber, P., Continuous Paranematic-to-Nematic Ordering Transitions of Liquid Crystals in Tubular Silica Nanochannels. *Physical Review Letters* **2008,** *101* (18), 187801.

21. Morineau, D.; Alba-Simionesco, C., Does Molecular Self-Association Survive in Nanochannels? *Journal of Physical Chemistry Letters* **2010,** *1* (7), 1155-1159.

22. Richert, R., Dynamics of Nanoconfined Supercooled Liquids. *Annual Review of Physical Chemistry, Vol 62* **2011,** *62*, 65-84.

23. Huber, P., Soft Matter in Hard Confinement: Phase Transition Thermodynamics, Structure, Texture, Diffusion and Flow in Nanoporous Media. *Journal of Physics-Condensed Matter* **2015,** *27* (10).

24. Krycka, K.; Dura, J.; Langston, L.; Burba, C., Nanoconfinement-Induced Phase Segregation of Binary Benzene-Cyclohexane Solutions within a Chemically Inert Matrix. *Journal of Physical Chemistry C* **2018,** *122* (14), 7676-7684.

25. Meissner, J.; Prause, A.; Findenegg, G., Secondary Confinement of Water Observed in Eutectic Melting of Aqueous Salt Systems in Nanopores. *Journal of Physical Chemistry Letters* **2016,** *7* (10), 1816-1820.

26. Burba, C.; Janzen, J., Confinement Effects on the Phase Transition Temperature of Aqueous NaCl Solutions: The Extended Gibbs-Thomson Equation. *Thermochimica Acta* **2015,** *615*, 81-87.

27. Ito, Y.; Miyaoka, T.; Tomita, N.; Yoshimi, T.; Sugimoto, T.; Takemura, T.; Nagoe, A.; Fujimori, H., Freezing-point Depression of Benzene Confined in Mesoporous Silica SBA-15 on Doping with a Slight Amount of Toluene: Ideal Behavior in a Nanometer-sized Space. *Chemistry Letters* **2017,** *46* (3), 296-298.

28. Jantsch, E.; Weinberger, C.; Tiemann, M.; Koop, T., Phase Transitions of Ice in Aqueous Salt Solutions within Nanometer-Sized Pores. *Journal of Physical Chemistry C* **2019,** *123* (40), 24566-24574.

29. Ediger, M. D.; Angell, C. A.; Nagel, S. R., Supercooled Liquids and Glasses. *Journal of Physical Chemistry* **1996,** *100* (31), 13200-13212.

30. Busselez, R.; Lefort, R.; Guendouz, M.; Frick, B.; Merdrignac-Conanec, O.; Morineau, D., Molecular Dynamics of Glycerol and Glycerol-Trehalose Bioprotectant Solutions Nanoconfined in Porous Silicon. *Journal of Chemical Physics* **2009,** *130* (21), 214502.

31. Busselez, R.; Lefort, R.; Ghoufi, A.; Beuneu, B.; Frick, B.; Affouard, F.; Morineau, D., The non-Gaussian Dynamics of Glycerol. *Journal of Physics-Condensed Matter* **2011,** *23* (50).

32. Lane, L., Freezing Points of Glycerol and its Aqueous Solutions. *Industrial and Engineering Chemistry* **1925,** *17*, 924-924.

33. Murthy, S.; Singh, G., Examination of the Concentration Dependence of T-g of Binary Aqueous Solutions. *Thermochimica Acta* **2008,** *469* (1-2), 116-119.

34. Bachler, J.; Fuentes-Landete, V.; Jahn, D.; Wong, J.; Giovambattista, N.; Loerting, T., Glass Polymorphism in Glycerol-Water Mixtures: II. Experimental Studies. *Physical Chemistry Chemical Physics* **2016,** *18* (16), 11058-11068.

35. Bachler, J.; Handle, P.; Giovambattista, N.; Loerting, T., Glass Polymorphism and Liquid-Liquid Phase Transition in Aqueous Solutions: Experiments and Computer Simulations. *Physical Chemistry Chemical Physics* **2019,** *21* (42), 23238-23268.

36. Zhao, L.; Cao, Z.; Wang, Q., Glass Transition of Aqueous Solutions Involving Annealing-Induced Ice Recrystallization Resolves Liquid-Liquid Transition Puzzle of Water. *Scientific Reports* **2015,** *5*.

37. Popov, I.; Greenbaum, A.; Sokolov, A.; Feldman, Y., The Puzzling First-Order Phase Transition in Water-Glycerol Mixtures. *Physical Chemistry Chemical Physics* **2015,** *17* (27), 18063-18071.

38. Findenegg, G. H.; Jahnert, S.; Akcakayiran, D.; Schreiber, A., Freezing and Melting of Water Confined in Silica Nanopores. *Chemphyschem* **2008,** *9* (18), 2651-2659.

39. Elamin, K.; Jansson, H.; Kittaka, S.; Swenson, J., Different Behavior of Water in Confined Solutions of High and Low Solute Concentrations. *Physical Chemistry Chemical Physics* **2013,** *15* (42), 18437-18444.

40. Schawe, J., A Quantitative DSC Analysis of the Metastable Phase Behavior of the Sucrose-Water System. *Thermochimica Acta* **2006,** *451* (1-2), 115-125.

41. Jani, A.; Sohier, T.; Morineau, D., Phase behavior of aqueous solutions of ethaline deep eutectic solvent. *Journal of Molecular Liquids* **2020,** *304*.

42. Thangswamy, M.; Maheshwari, P.; Dutta, D.; Bera, A. K.; Singh , M. N.; Sinha, A. K.; Yusuf, S. M.; Pujari, P. K., Evolution of confined ice nano structures at different levels of

pore filling: a synchrotron based X-ray diffraction study. *Physical Chemistry Chemical Physics* **2020,** *Advance Article*.

43. Johari, G. P.; Fleissner, G.; Hallbrucker, A.; Mayer, E., Thermodynamic Continuity between Glassy and Normal Water. *Journal of Physical Chemistry* **1994,** *98* (17), 4719-4725.

44. Nakagawa, H.; Oyama, T., Molecular Basis of Water Activity in Glycerol-Water Mixtures. *Frontiers in Chemistry* **2019,** *7*.

45. Koop, T.; Luo, B. P.; Tsias, A.; Peter, T., Water Activity as the Determinant for Homogeneous Ice Nucleation in Aqueous Solutions. *Nature* **2000,** *406* (6796), 611-614.

46. Hamid, A. R. A.; Mhanna, R.; Catrou, P.; Bulteau, Y.; Lefort, R.; Morineau, D., Multiple Glass Transitions of Microphase Separed Binary Liquids Confined in MCM-41. *Journal of Physical Chemistry C* **2016,** *120* (20), 11049-11053.

47. Swenson, J.; Elamin, K.; Chen, G.; Lohstroh, W.; Sakai, V. G., Anomalous Dynamics of Aqueous Solutions of di-Propylene Glycol Methylether Confined in MCM-41 by Quasielastic Neutron Scattering. *Journal of Chemical Physics* **2014,** *141* (21).

48. Sattig, M.; Elamin, K.; Reuhl, M.; Swenson, J.; Vogel, M., Dynamics of DiPGME-Water Mixtures in Mesoporous Silica. *Journal of Physical Chemistry C* **2017,** *121* (12), 6796-6806.

49. Hamid, A. R. A.; Mhanna, R.; Lefort, R.; Ghoufi, A.; Alba-Simionesco, C.; Frick, B.; Morineau, D., Microphase Separation of Binary Liquids Confined in Cylindrical Pores. *Journal of Physical Chemistry C* **2016,** *120* (17), 9245-9252.

50. Mhanna, R.; Hamid, A.; Dutta, S.; Lefort, R.; Noirez, L.; Frick, B.; Morineau, D., More Room for Microphase Separation: An Extended Study on Binary Liquids Confined in SBA-15 Cylindrical Pores. *Journal of Chemical Physics* **2017,** *146* (2).

51. Essafri, I.; Morineau, D.; Ghoufi, A., Microphase Separation of a Miscible Binary Liquid Mixture under Confinement at the Nanoscale. *Npj Computational Materials* **2019,** *5*.

52. Demuth, D.; Sattig, M.; Steinrucken, E.; Weigler, M.; Vogel, M., H-2 NMR Studies on the Dynamics of Pure and Mixed Hydrogen-Bonded Liquids in Confinement. *Zeitschrift Fur Physikalische Chemie-International Journal of Research in Physical Chemistry & Chemical Physics* **2018,** *232* (7-8), 1059-1087.

Supporting Information: Extension and Limits of Cryoscopy for Nanoconfined Solutions

Benjamin Malfait,[†] Alban Pouessel,[†] Aîcha Jani,[†] Denis Morineau[†*]

[†]Institute of Physics of Rennes, CNRS-University of Rennes 1, UMR 6251, F-35042 Rennes, France

Corresponding Author

* Email: denis.morineau@univ-rennes1.fr

1. Phase Diagram and thermograms of Bulk Glycerol-Water Solutions

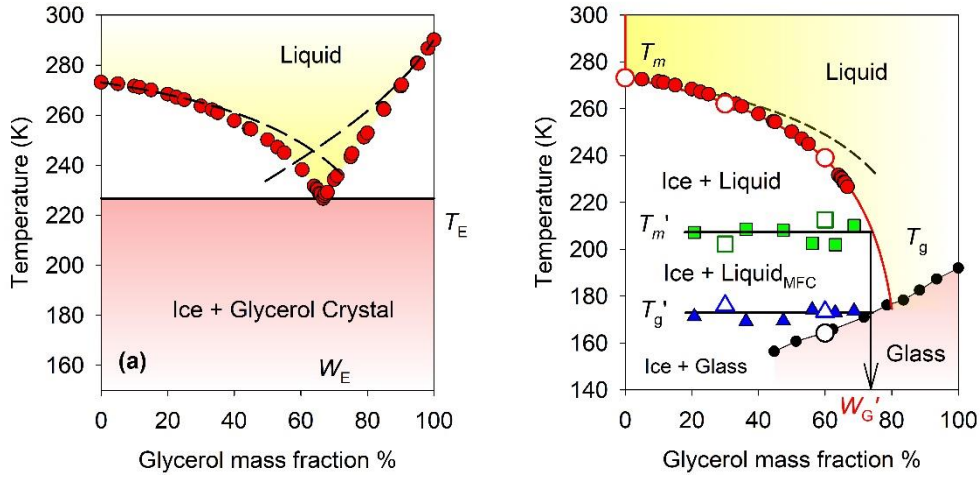

Figure S1. Phase diagram of the glycerol – water binary mixture as a function of the mass fraction of glycerol. (a) Glycerol crystallization was induced by seeding. The experimental equilibrium liquidus lines (filled circles) and eutectic point (T_E) are from ref. 1. (b) Glycerol did not crystallize (metastable region). The glass transition temperatures of the homogenous aqueous solution T_g (black filled circles) from ref. 2, those of the maximally freeze concentrated solution T_g' (filled triangles) and the onset of melting of ice in the maximally freeze-concentrated solution T_m' (filled squares) are from ref. 3. The values obtained from this study (open symbols). The theoretical predictions from ideal mixing are illustrated as dashed lines. Solid lines are guides for the eyes. The composition of the maximally freeze-concentrated solution (W_G') is indicated by the intercept between T_g' and T_g.

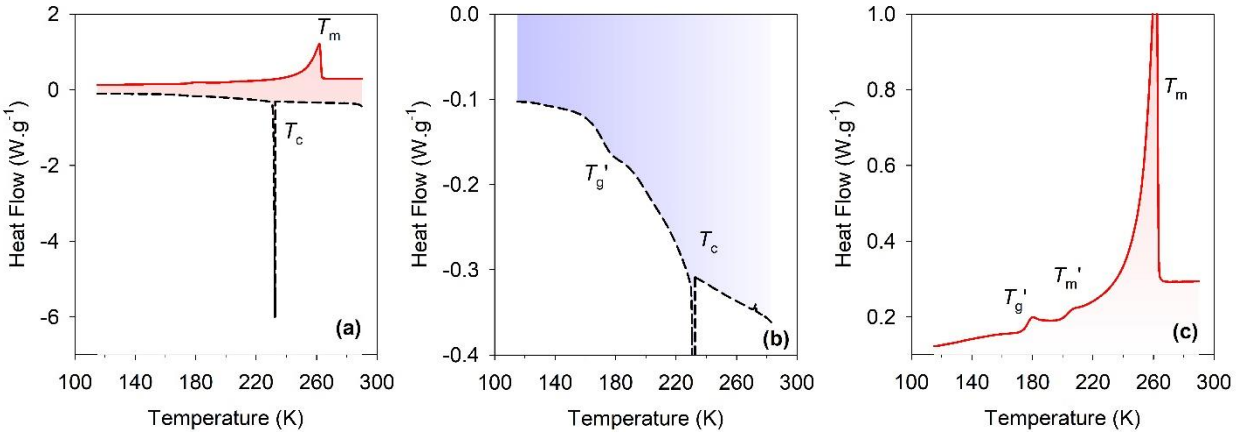

Figure S2. Thermogram of the bulk glycerol solution (W_G = 30%). (a) A first cooling ramp from 290K to 110K (black dashed line) and heating (red solid line), (b) and (c) magnified views of the cooling and heating branches, respectively.

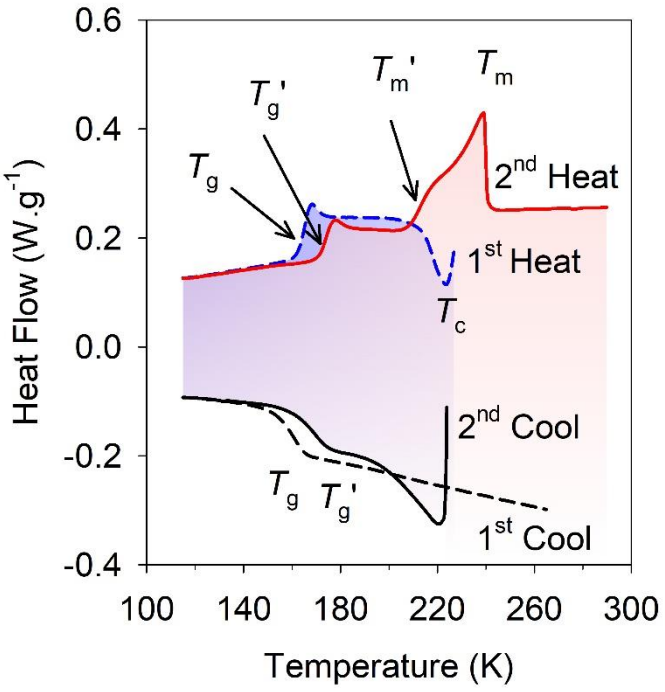

Figure S3. Thermogram of the bulk glycerol solution (W_G = 60%) with application of a specific thermal cycling. A first cooling ramp from 290K to 110K (black dashed line) presents a liquid-to-glass transition at T_g, a subsequent first heating ramp up to 227K (blue dashed line) presents a glass-to-liquid transition followed by crystallization (T_c), a second cooling branch down to 110K (black solid line) presents a liquid-to-glass transition of the maximally-freeze-concentrated solution at T_g', and a final heating ramp up to 290K (red solid line) presents the glass-to-liquid transition of the maximally-freeze-concentrated solution at T_g', followed by a broad melting peak (onset of melting T_m' and maximum T_m located at the liquidus).

2. DSC Thermograms, and Melting Enthalpy of confined Glycerol-Water Solutions

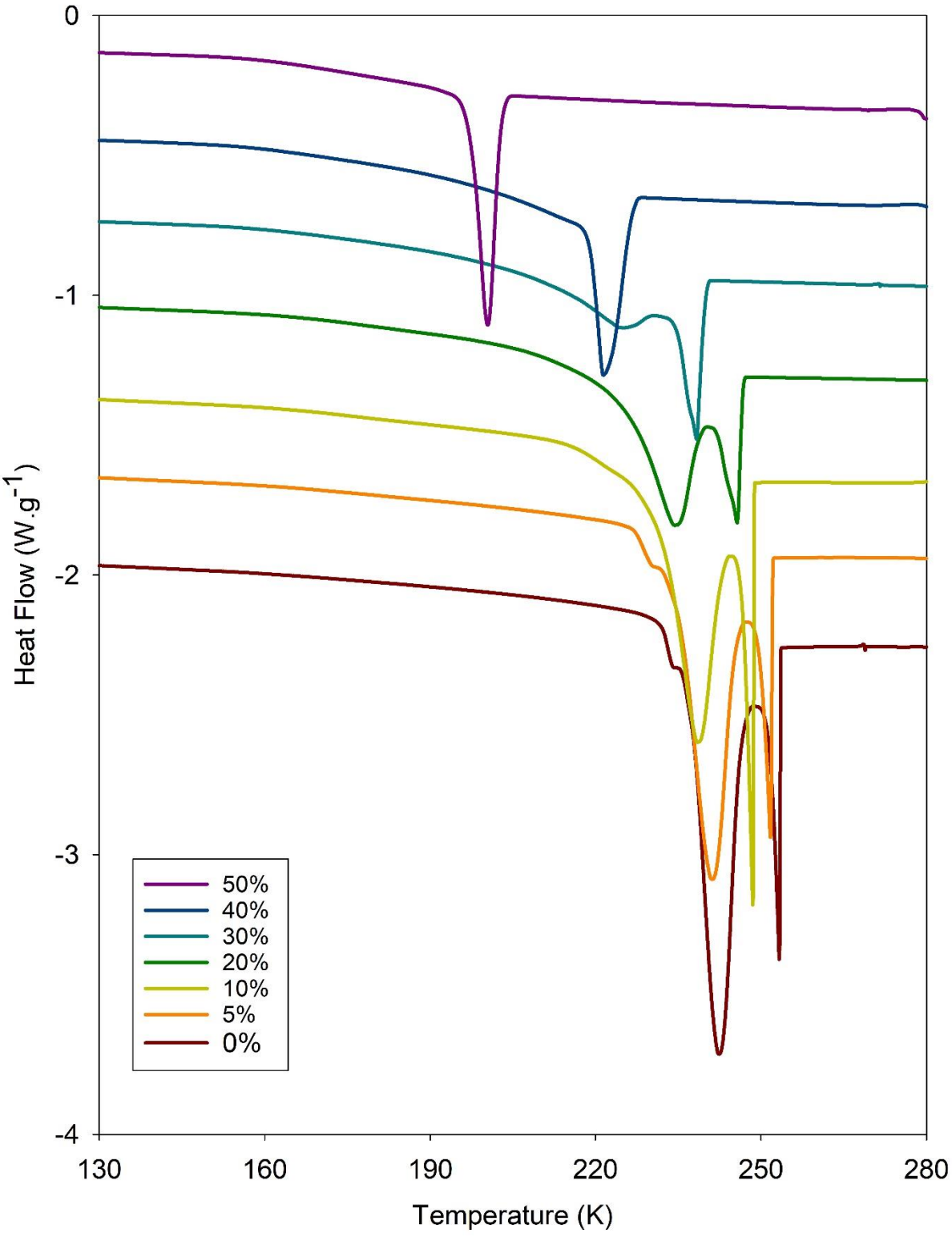

Figure S4 Thermograms of the glycerol solution confined in SBA-15 during cooling from 290 to 115K. For glycerol mass fractions ranging from 0 to 50% from bottom to top. Curves are vertically shifted by 0.3 for better clarity.

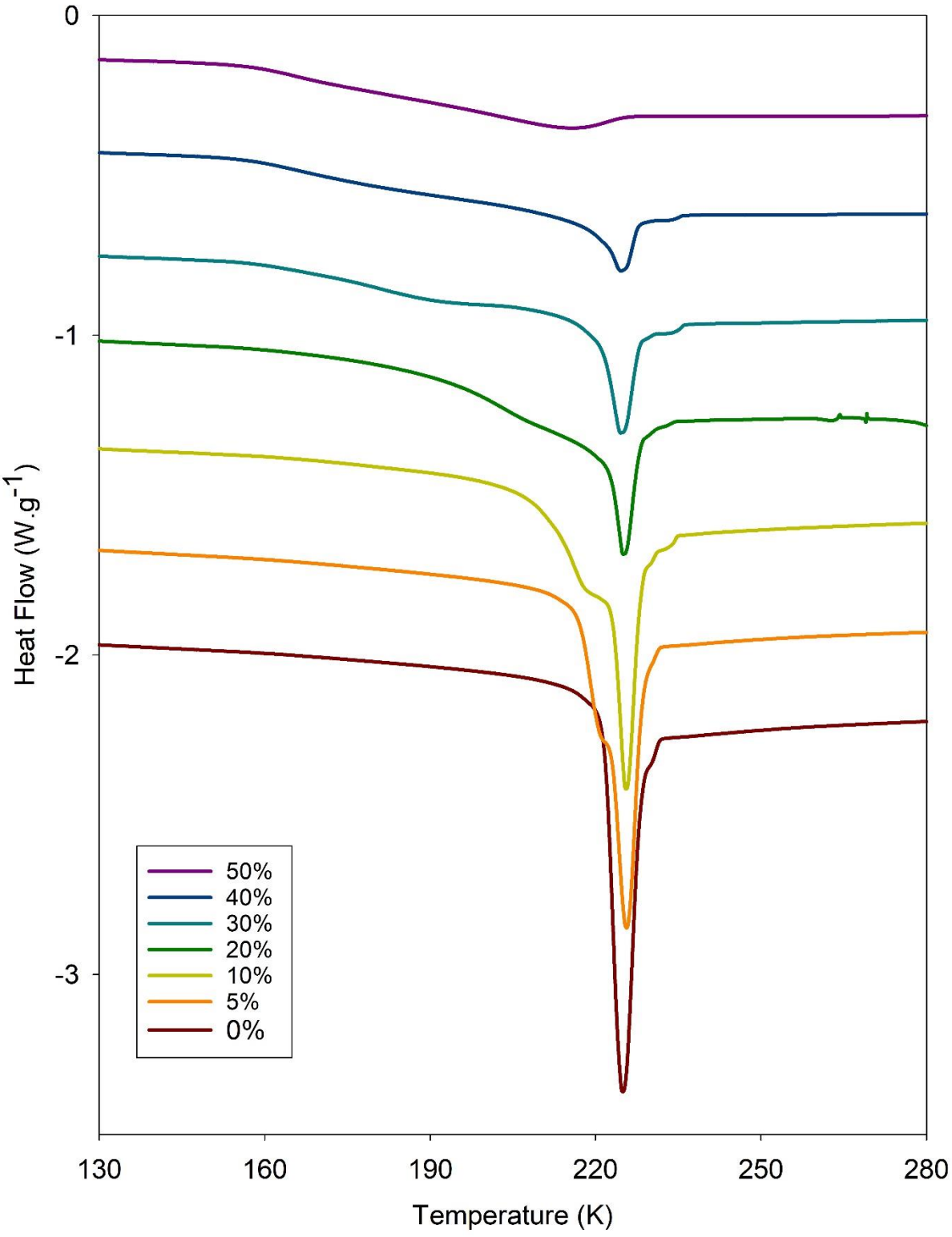

Figure S5 Thermograms of the glycerol solution confined in MCM-41 during cooling from 290 to 155K. For glycerol mass fractions ranging from 0 to 50% from bottom to top. Curves are vertically shifted by 0.3 for better clarity.

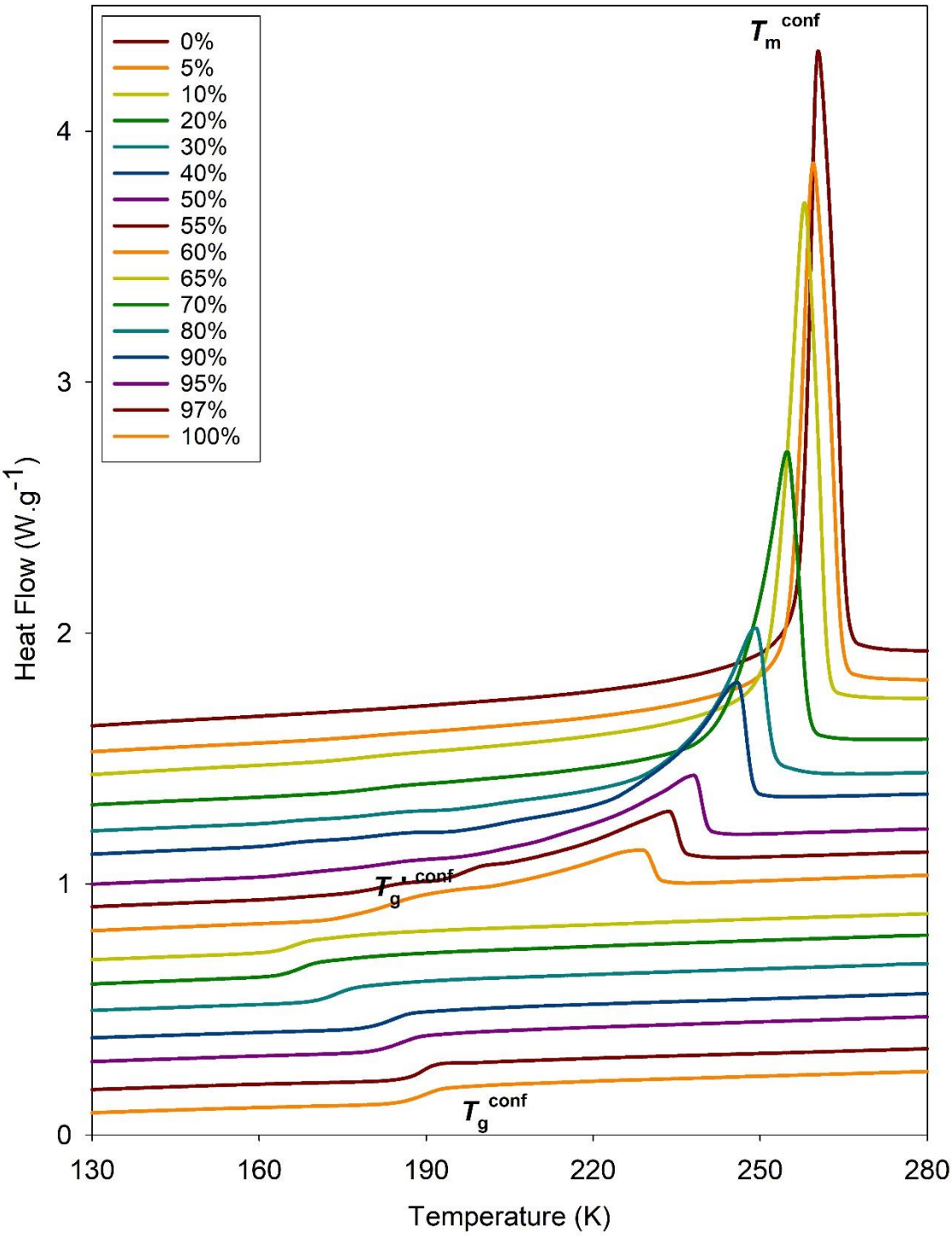

Figure S6. Thermograms of the glycerol solution confined in SBA-15 during heating from 115 to 290K. Glycerol mass fractions ranging from 0 to 100% from top to bottom. Curves are vertically shifted by 0.1 for better clarity.

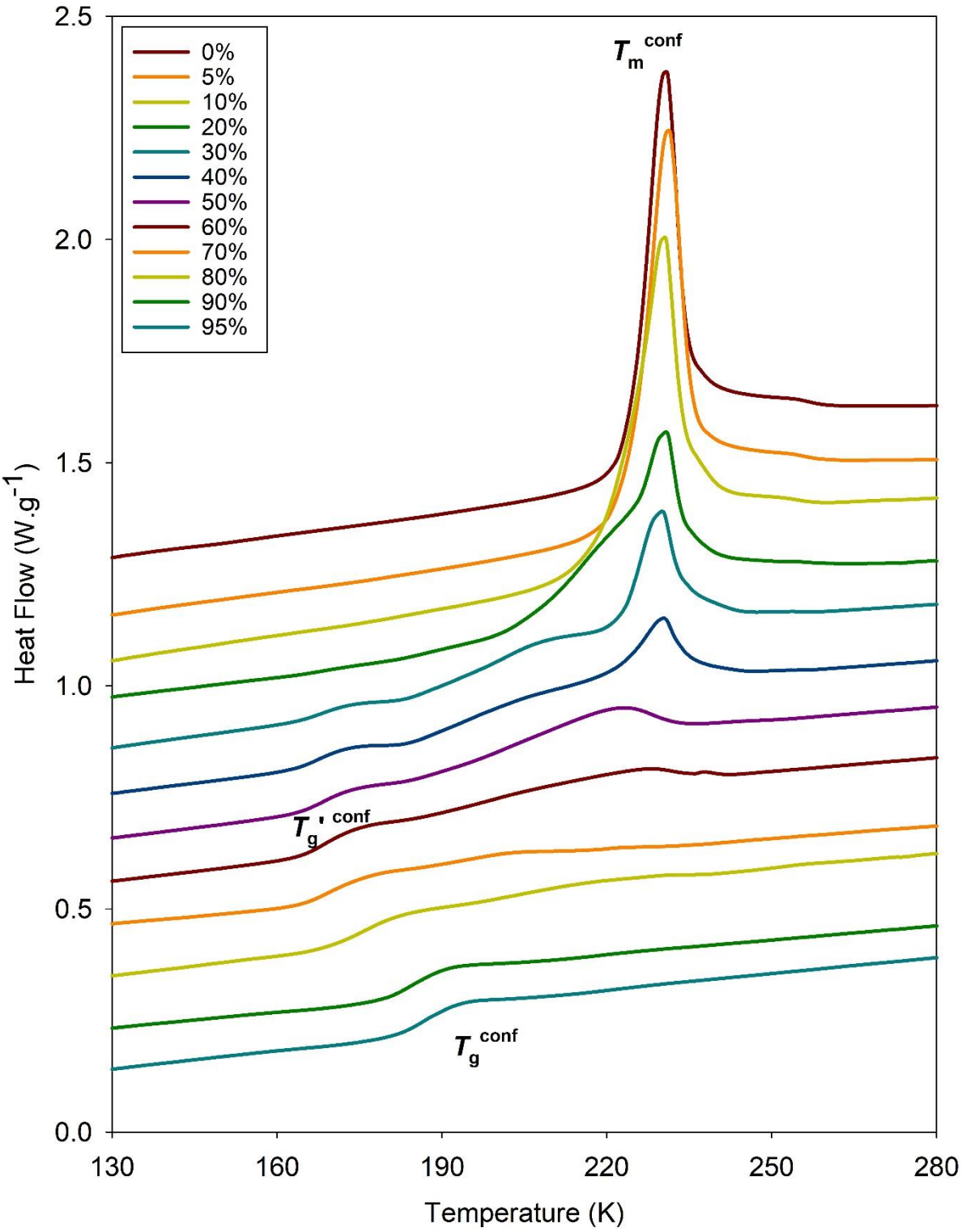

Figure S7. Thermograms of the glycerol solution confined in MCM-41 during heating from 115 to 290K. Glycerol mass fractions ranging from 0 to 95% from top to bottom. Curves are vertically shifted by 0.1 for better clarity.

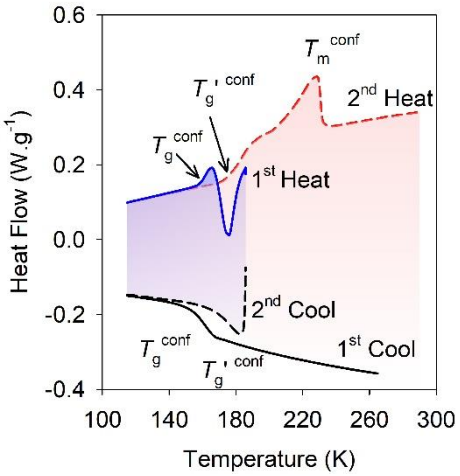

Figure S8. Thermogram of the glycerol solution confined in SBA-15 (W_G = 60%) with application of a specific thermal cycling. A first cooling ramp from 290K to 115K (black solid line) presents a liquid-to-glass transition at T_g^{conf}, a subsequent first heating ramp up to 186K (blue solid line) presents a glass-to-liquid transition followed by crystallization, a second cooling branch down to 115K (black dashed line) presents a liquid-to-glass transition of the maximally-freeze-concentrated solution at $T_g^{'conf}$, and a final heating ramp up to 290K (red dashed line) presents a broad melting peak.

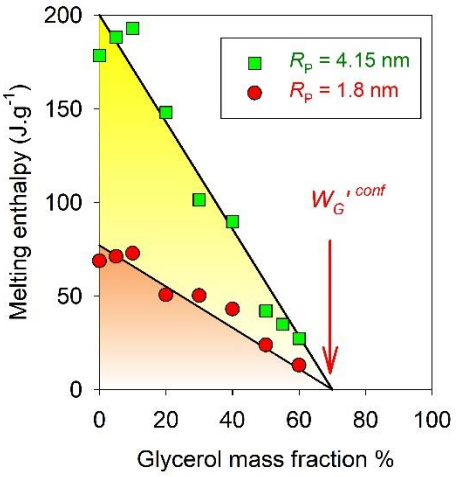

Figure S9. Ice melting enthalpy of the glycerol solutions confined in SBA-15 (green squares) and MCM-41 (red circles) as a function of the glycerol mass fraction W_G. The enthalpy was normalized with respect to the mass of the glycerol solution.

3. Theoretical Models.

The Gibbs energy of a crystal of ice, composed of n_s water molecules, occupying a cylindrical volume with radius *r* and length *L* being contact with a solution of molar concentration *x* writes as

$$G_s(T, n_s) = n_s\mu_s(T) + 2\pi r L\gamma_{sl} + 2\pi r^2\gamma_{sl} \qquad \text{(S1)}$$

where $\mu_s(T)$ is the chemical potential of water in ice and γ_{sl} the ice-solution surface energy.

One notes that

$$n_s = \frac{\pi L r^2}{v_s} \qquad \text{(S2)}$$

where $v_s$is the molar volume of water in ice.

From (S1) and (S2) one gets

$$G_s(T, n_s) = n_s\mu_s(T) + 2\frac{n_s v_s}{r}\gamma_{sl} + 2\pi r^2\gamma_{sl} \qquad \text{(S3)}$$

The melting temperature T_r^x of the confined ice of radius *r* located in a solution of solute molar fraction *x* is determined by the equilibrium condition between the solid and the liquid phases, which implies that

$$\left(\frac{\partial G_s}{\partial n_s}\right) = \left(\frac{\partial G_l}{\partial n_l}\right) \qquad \text{(S4)}$$

with n_l and G_l being respectively the number of water molecules and the total Gibbs energy of the solution that is in equilibrium with the ice crystal. If *r* is supposed constant, and by definition of $\mu_l(T,x)$, the chemical potential of water in the liquid solution, one gets

$$\mu_s(T_r^x) + 2\frac{v_s}{r}\gamma_{sl} = \mu_l(T_r^x, x) \quad \text{(S5)}$$

$$\mu_s(T_r^x) - \mu_l(T_r^x, x) = -\frac{2\,v_s\gamma_{sl}}{r} \quad \text{(S6)}$$

The activity of water in a glycerol liquid solution of molar fraction *x* confined in a pore of radius *r*, at the temperature T_r^x is defined by

$$\mu_l(T_r^x, x) = \mu_l(T_r^x, x = 0) + RT_r^x \ln(a(r, T_r^x, x)) \quad \text{(S7)}$$

where *R* is the gas constant.

Introducing (S7) in (S6) one gets

$$\mu_s(T_r^x) - \mu_l(T_r^x, x = 0) - RT_r^x \ln(a(r, T_r^x, x)) = -\frac{2\,v_s\gamma_{sl}}{r} \quad \text{(S8)}$$

For the pure confined liquid, on gets

$$\mu_s(T_r^0) - \mu_l(T_r^0, x = 0) = -\frac{2\,v_s\gamma_{sl}}{r} = -\frac{2\,v_s\gamma_{sl}}{R_p - e} \quad \text{(S9)}$$

where T_r^0 is the melting temperature of ice for pure water confined in a pore a radius R_p, and *e* is the thickness of the unfrozen liquid layer, so that $r = R_p - e$.

For the bulk pure liquid, one gets

$$\mu_s(T_{bulk}^0) - \mu_l(T_{bulk}^0, x = 0) = 0 \quad \text{(S10)}$$

where $T_{bulk}^0$is the melting temperature of bulk pure water.

For the general case of a confined solution (i.e. eq. S8), it is needed to evaluate, $\mu_s(T_r^x) - \mu_l(T_r^x, x = 0)$, which is the difference between the chemical potential of pure bulk water in the solid and the liquid states. It could be evaluated by thermodynamical integration between T_{bulk}^0 where it vanishes cf. (S10) and T_r^x, noting that for a pure system, the Gibbs-Helmholtz relation applies

i.e. $\left(\frac{\partial\left(\frac{\Delta\mu}{T}\right)}{\partial T}\right) = \frac{-\Delta h}{T^2}$, with $\Delta\mu$ and Δh being the difference in the chemical potential and molar enthalpy between ice and pure liquid water.

This integration requires a precise knowledge of the temperature variation of the heat capacity of liquid water and ice on a broad temperature range. It has been measured experimentally by DSC by Johari in a temperature range from 273,15 to 153K.[5] The obtained results were later parametrized by Koop *at al.*[6], as follows:

$$\Delta\mu_0(T) = \mu_s(T) - \mu_l(T, x = 0) = 210368 + 131.438\,T\ - 3.32373\,.10^6\,T^{-1} - 41729.1\ln(T) \qquad \text{(S11)}.$$

Neglecting the temperature influence on the heat capacities, classical thermodynamics integration can also be used to give an approximated estimate of $\Delta\mu_0(T)$:

$$\Delta\mu_0(T) = -\Delta H_m\left(1 - \frac{T}{T_{bulk}^0}\right) - \Delta C_p(T - T_{bulk}^0) + \Delta C_p T ln\left(\frac{T}{T_{bulk}^0}\right) \qquad \text{(S12)}$$

with ΔH_m and ΔC_p being respectively the molar melting enthalpy and molar heat capacity difference between liquid and ice at the melting point of pure water T_{bulk}^0.

The later equation can be even more simplified, by considering only the first dominant term as :

$$\widehat{\Delta\mu_0}(T) = -\Delta H_m \left(1 - \frac{T}{T_{bulk}^0}\right) \quad \text{(S13)}$$

Then introducing (S11) in (S8) gives:

$$\Delta\mu_0(T_r^x) - RT_r^x \ln(a(r, T_r^x, x)) = -\frac{2\,v_s\gamma_{sl}}{r} \quad \text{(S14)}$$

Which for the pure confined water is

$$\Delta\mu_0(T_r^0) = -\frac{2\,v_s\gamma_{sl}}{r} \quad \text{(S15)}$$

Then assuming that γ_{sl} does not vary with *x* and *T*, subtracting (S15) and (S14) gives

$$\Delta\mu_0(T_r^x) - \Delta\mu_0(T_r^0) - RT_r^x \ln(a(r, T_r^x, x)) = 0 \quad \text{(S16)}$$

If the limit case of ideal **mixing approximation** is assumed, *i.e.* $a(r, T_r^x, x) = (1 - x)$

(S16) becomes

$$\Delta\mu_0(T_r^x) - \Delta\mu_0(T_r^0) - RT_r^x \ln(1 - x) = 0 \quad \text{(S17)}$$

which allows predicting the cryoscopic melting point depression in confined environment.

If $\widehat{\Delta\mu_0}$ (S13) instead of $\Delta\mu_0$ (S11) is used to further approximate the chemical potential of pure bulk water, then (S14) writes as (S18), which leads to the **extended Gibbs-Thomson equation** (S19) as illustrated as dashed line in Figure 2 :

$$-\Delta H_m \left(1 - \frac{T_r^x}{T_{bulk}^0}\right) - RT_r^x \ln(1 - x) = -\frac{2\,v_s\gamma_{sl}}{r} \quad \text{(S18)}$$

$$T_r^x - T_{bulk}^0 = \frac{-2v_s\gamma_{sl}T_{bulk}^0}{\Delta H_m r} + \frac{RT_r^x\, T_{bulk}^0 \ln(1-x)}{\Delta H_m} \qquad \text{(S19)}$$

For the pure confined water ($x = 0$), the latter gives the **classical Gibbs-Thomson equation**:

$$T_r^0 - T_{bulk}^0 = \frac{-2v_s\gamma_{sl}T_{bulk}^0}{\Delta H_m r} \qquad \text{(S20)}$$

and for the bulk solution, it gives the **classical cryoscopic equation for ideal mixing**

$$\frac{1}{T_{bulk}^x} - \frac{1}{T_{bulk}^0} = -\frac{R\ln(1-x)}{\Delta H_m} \qquad \text{(S21)}$$

Combining the extended Gibbs-Thomson equation for the aqueous solution (S19), and Gibbs-Thomson equation for the pure water (S20) and one can remove explicit reference to the pore size and surface tension, and one gets

$$T_r^x = T_r^0 + \frac{RT_r^x\, T_{bulk}^0 \ln(1-x)}{\Delta H_m} \qquad \text{(S22)}$$

and so the **extended cryoscopic equation for ideal mixing**

$$\frac{1}{T_r^x} - \frac{1}{T_r^0} = -\left(\frac{T_{bulk}^0}{T_r^0}\right)\frac{R\ln(1-x)}{\Delta H_m} \qquad \text{(S23)}$$

The predictions from this extended cryoscopic equation for ideal mixing are illustrated as short dashed lines in Figure 4.

In order to quantify the extent of the **deviation from the ideal mixing**, one can calculate the actual activity of water in the confined mixtures using the experimental values of the melting temperatures by simple transformation of equation (S16), which gives

$$a(r, T_r^x, x) = Exp\left\{\frac{\Delta\mu_0(T_r^x) - \Delta\mu_0(T_r^0)}{R\, T_r^x}\right\} \qquad \text{(S24)}$$

and for bulk liquid

$$a(r, T_{bulk}^{x}, x) = Exp\left\{\frac{\Delta\mu_0(T_{bulk}^{x})}{RT_{bulk}^{x}}\right\} \quad \text{(S25)}$$

(S24) and (S25) allowed us to evaluate the water activity from the experimental melting points, as shown in Figure 5.

Table 1. Melting Point of Confined Pure Water[a]

Pore radius R (nm)	Experimental melting point T_m^{conf} (K)	Theoretical melting point T_m^{conf} (K)
4.15	260.4	258.5
1.8	230.2	229.9

[a]The value of the Gibbs-Thomson constant $C_{GT} = \frac{2\gamma_{sl}T^0_{bulk}}{\Delta H_m \rho_s} = 52.4\ K.nm$ and the thickness of the unfreezable water layer e = 0.6 nm was used from Findennegg at al.[7]

Notations :

r : radius of the confined ice

R_p : pore radius

e : thickness of the interfacial liquid layer

v_s : molar volume of ice

γ_{sl} : ice-liquid surface energy

L : length of the confined ice

$\mu_s(T)$: chemical potential ice at temperature T

$\mu_l(T,x)$: chemical potential of the solution of composition x at temperature T

$\Delta\mu_0(T)$: difference of chemical potential between solid and liquid pure bulk water at temperature T.

T^0_{bulk} : melting temperature of bulk pure water

4. Materials and Methods

4.1. Samples. Glycerol (>99%) were purchased from Sigma-Aldrich and used directly, without further purification. A series of working aqueous solutions of glycerol (~5ml each) were prepared by pipetting and addition of deionized water to glycerol. The appropriate value of the composition (in glycerol weight fraction) was checked by measuring the mass at each stage of the preparation. Aqueous solutions were mixed by mechanical agitation until a clear homogeneous liquid phase was obtained and served as stock solutions for the confined systems.

The mesoporous materials MCM-41 silicates were prepared in our laboratory according to a procedure similar to that described elsewhere[8] and already used in previous works.[9,10,11,12] Hexadecyl-ammonium bromide was used as template to get a mesostructured triangular array of aligned channels with pore diameter D = 3.65 nm, and porous volume V_P = 0.665 cm^3 g^{-1}. The SBA-15 mesoporous silicates were prepared using a procedure described elsewhere,[9, 13-16] with slight modifications of the thermal treatments to optimize the final structure of the product.[17] Nonionic triblock copolymer (Pluronic P_{123}): $(EO)_{20}(PO)_{70}(EO)_{20}$ was used as a template to obtain a mesostructured triangular array of aligned channels with a pore diameter D = 8.3 nm, and porous volume V_P = 1.0 cm^3 g^{-1}.

Pore size and porous volume were assessed by nitrogen adsorption, and the overall regular porous structure of both matrices were confirmed by transmission electron microscopy and neutron diffraction.

The calcined matrices were dried at 120°C under primary vacuum for 12 hours prior to the experiments. The empty MCM-41 and SBA-15 were packed in DSC Tzero© aluminum hermetic pans and then filled by liquid imbibition with the appropriate weighted amount of

glycerol aqueous mixtures (typically 3-4mg) injected from a syringe to allow complete loading of the porous volume (filling fraction 90-100%). They were then hermetically sealed in the aluminum pans and their masses measured with a microbalance.

DSC experiments have concluded to the absence of bulk ice crystallization. They indicate that no bulk excess liquid is present out of the matrix, and that the porosity is therefore completely filled, in agreement with previous studies using the same filling method (cf. control of the filling fraction).[9,11,12]

4.2. DSC Experiments. The differential scanning calorimetry (DSC) measurements were performed with a Q-20 TA Instrument equipped with a liquid nitrogen cooling system. The melting transition of an indium sample was used for calibration of temperature and heat flux. The accuracy of the calibration was checked by measuring the melting of pure ice that gave Tm=213.17K, ΔH_m=310 $J.g^{-1}$. The thermograms were recorded with a linear temperature ramp on cooling and heating in the temperature range from 110 to 300K (scanning rate of 5 $K.min^{-1}$).

4.3. Control of the filling fraction

It is important to note that the control of the filling fraction with no reservoir of excess liquid was confirmed by the absence of additional endothermic peak for all thermograms that would have indicated the melting of a hypothetical excess of water. Moreover, we could demonstrate with samples in which a small amount of excess solution was intentionally used that the excess liquid was detected by an additional peak, precisely located at the bulk melting temperature (cf. Figures S10a and S10b). In addition, we confirmed that in the presence of excess liquid, the melting peak attributed to the confined solution was indeed shifted down to lower temperature (by about 2 K for *W*=30%, and 7 K for *W*=60%) as illustrated in Figures S11a and S11b. This

effect clearly indicates that the composition of the confined solution differs from the initial one when a reservoir of excess liquid is used. This is consistent with the observed phenomena and the experimental limitations encountered in the literature and discussed in the introductory part of the Letter.

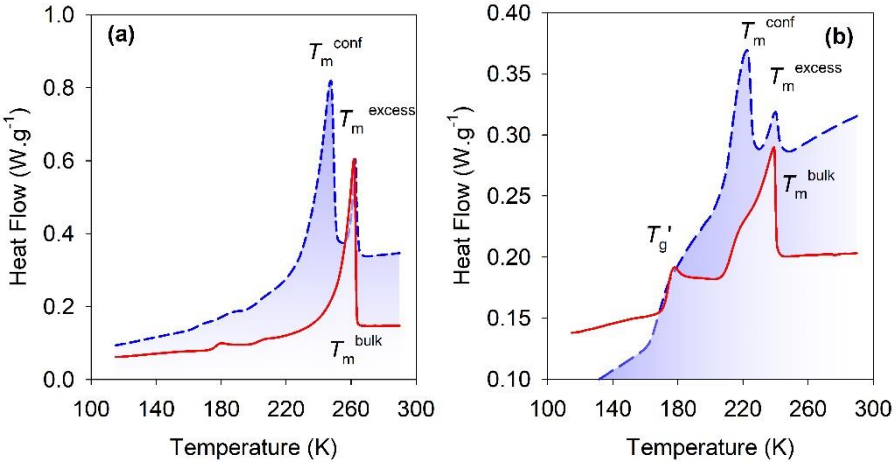

Figure S10. Thermogram during heating of the crystallized bulk solution (red solid line) and confined in SBA-15 (blue dashed line) with an external reservoir of bulk excess liquid. Mass fraction of glycerol (a) W_G = 30% and (b) W_G = 60%. The thermograms of the bulk solutions are scaled x0.5 for better clarity.

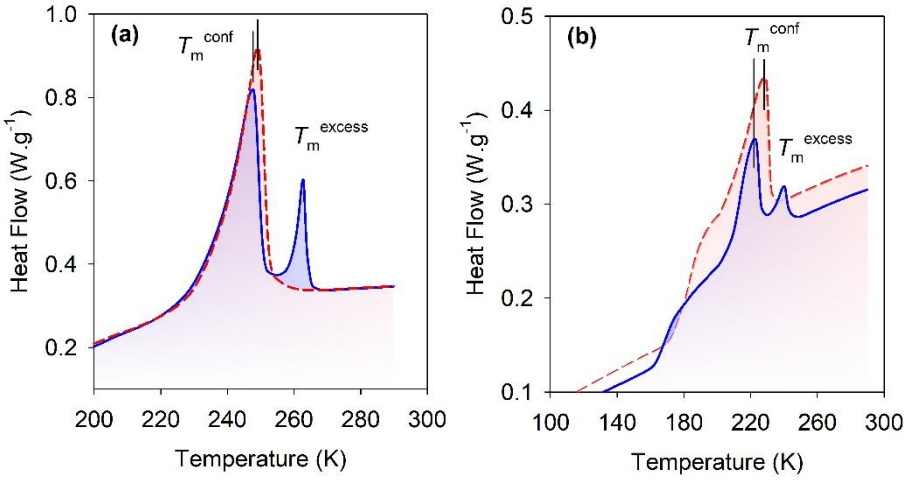

Figure S11. Thermogram during heating of the crystallized solution confined in SBA-15 without (red dashed line) or with (blue solid line) an external reservoir of bulk excess liquid. Mass fraction of glycerol (a) W_G = 30% and (b) W_G = 60%. The vertical solid lines indicate the downward shift of the melting peak of the confined solution due to the presence of a reservoir of excess liquid.

5. References

1. Lane, L., Freezing Points of Glycerol and its Aqueous Solutions. *Industrial and Engineering Chemistry* **1925,** *17*, 924-924.

2. Murthy, S.; Singh, G., Examination of the Concentration Dependence of T-g of Binary Aqueous Solutions. *Thermochimica Acta* **2008,** *469* (1-2), 116-119.

3. Bachler, J.; Fuentes-Landete, V.; Jahn, D.; Wong, J.; Giovambattista, N.; Loerting, T., Glass Polymorphism in Glycerol-Water Mixtures: II. Experimental Studies. *Physical Chemistry Chemical Physics* **2016,** *18* (16), 11058-11068.

4. Bachler, J.; Handle, P.; Giovambattista, N.; Loerting, T., Glass Polymorphism and Liquid-Liquid Phase Transition in Aqueous Solutions: Experiments and Computer Simulations. *Physical Chemistry Chemical Physics* **2019,** *21* (42), 23238-23268.

5. Johari, G. P.; Fleissner, G.; Hallbrucker, A.; Mayer, E., Thermodynamic Continuity between Glassy and Normal Water. *Journal of Physical Chemistry* **1994,** *98* (17), 4719-4725.

6. Koop, T.; Luo, B. P.; Tsias, A.; Peter, T., Water Activity as the Determinant for Homogeneous Ice Nucleation in Aqueous Solutions. *Nature* **2000,** *406* (6796), 611-614.

7. Findenegg, G. H.; Jahnert, S.; Akcakayiran, D.; Schreiber, A., Freezing and Melting of Water Confined in Silica Nanopores. *Chemphyschem* **2008,** *9* (18), 2651-2659.

8. Grun, M.; Lauer, I.; Unger, K. K., The Synthesis of Micrometer- and Submicrometer-Size Spheres of Ordered Mesoporous Oxide MCM-41. *Advanced Materials* **1997,** *9* (3), 254-&.

9. Alba-Simionesco, C.; Dosseh, G.; Dumont, E.; Frick, B.; Geil, B.; Morineau, D.; Teboul, V.; Xia, Y., Confinement of Molecular Liquids: Consequences on Thermodynamic, Static and Dynamical Properties of Benzene and Toluene. *European Physical Journal E* **2003,** *12* (1), 19-28.

10. Morineau, D.; Dosseh, G.; Alba-Simionesco, C.; Llewellyn, P., Glass Transition, Freezing and Melting of Liquids Confined in the Mesoporous Silicate MCM-41. *Philosophical Magazine B* **1999,** *79* (11-12), 1847-1855.

11. Morineau, D.; Xia, Y. D.; Alba-Simionesco, C., Finite-Size and Surface Effects on the Glass Transition of Liquid Toluene Confined in Cylindrical Mesopores. *Journal of Chemical Physics* **2002,** *117* (19), 8966-8972.

12. Morineau, D.; Guegan, R.; Xia, Y.; Alba-Simionesco, C., Structure of Liquid and Glassy Methanol Confined in Cylindrical Pores. *Journal of Chemical Physics* **2004,** *121* (3), 1466-1473.

13. Zhao, D.; Huo, Q.; Feng, J.; Chmelka, B.; Stucky, G., Nonionic Triblock and Star Diblock Copolymer and Oligomeric Surfactant Syntheses of Highly Ordered, Hydrothermally Stable, Mesoporous Silica Structures. *Journal of the American Chemical Society* **1998,** *120* (24), 6024-6036.

14. Audonnet, F.; Brodie-Linder, N.; Morineau, D.; Frick, B.; Alba-Simionesco, C., From the Capillary Condensation to the Glass Transition of a Confined Molecular Liquid: Case of Toluene. *Journal of Non-Crystalline Solids* **2015,** *407*, 262-269.

15. Dosseh, G.; Brodie-Linder, N.; Frick, B.; Le Quellec, C.; Morineau, D.; Alba-Simionesco, C., Dynamical Properties of Toluene and ortho-Terphenyl Confined in MCM-41 and SBA-15 Mesoporous Materials. *Annales De Chimie-Science Des Materiaux* **2005,** *30* (4), 365-373.

16. Xia, Y. D.; Dosseh, G.; Morineau, D.; Alba-Simionesco, C., Phase Diagram and Glass Transition of Confined Benzene. *Journal of Physical Chemistry B* **2006,** *110* (39), 19735-19744.

17. Brodie-Linder, N.; Dosseh, G.; Alba-Simonesco, C.; Audonnet, F.; Imperor-Clerc, M., SBA-15 synthesis: Are there Lasting Effects of Temperature Change within the First 10 min of TEOS Polymerization? *Materials Chemistry and Physics* **2008,** *108* (1), 73-81.